Coherent X-Ray Diffraction Imaging with Nanofocused Illumination

C. G. Schroer,[1] P. Boye,[1] J. M. Feldkamp,[1] J. Patommel,[1] A. Schropp,[1,3] A. Schwab,[1] S. Stephan,[1] M. Burghammer,[2] S. Schöder,[2] and C. Riekel[2]

[1]*Institute of Structural Physics, Technische Universität Dresden, D-01062 Dresden, Germany*
[2]*ESRF, B. P. 220, F-38043 Grenoble, France*
[3]*HASYLAB at DESY, Notkestr. 85, D-22607 Hamburg, Germany*

(Received 26 April 2008; published 29 August 2008)

Coherent x-ray diffraction imaging is an x-ray microscopy technique with the potential of reaching spatial resolutions well beyond the diffraction limits of x-ray microscopes based on optics. However, the available coherent dose at modern x-ray sources is limited, setting practical bounds on the spatial resolution of the technique. By focusing the available coherent flux onto the sample, the spatial resolution can be improved for radiation-hard specimens. A small gold particle (size <100 nm) was illuminated with a hard x-ray nanobeam ($E = 15.25$ keV, beam dimensions $\approx 100 \times 100$ nm^2) and is reconstructed from its coherent diffraction pattern. A resolution of about 5 nm is achieved in 600 s exposure time.

DOI: 10.1103/PhysRevLett.101.090801 PACS numbers: 07.85.Tt, 42.30.Rx, 78.70.Ck

Determining the structure of nanoscale objects, such as, for example, biomolecules in their cellular environment, small particles for industrial catalysis, and nanoelectronic devices, is crucial to understand their function and to push structural biology, chemistry, and nanotechnology to new frontiers. X-ray microscopy is well suited to investigate such systems [1], as it allows one to image them with high spatial resolution, with minimal sample preparation (e.g., shock-freezing), and inside environments for *in situ* studies, e.g., catalytic reactors or high magnetic fields. Currently, all direct x-ray microscopy techniques are limited in spatial resolution to a few 10 nm, due to aberrations and the limited numerical aperture of today's x-ray optics [2]. Coherent x-ray diffraction imaging (CXDI) does not rely on x-ray optics and, therefore, has the potential to push the spatial resolution limit to well beyond that of direct imaging techniques. In addition, x-ray free-electron lasers (XFELs) will provide ultra short and highly brilliant x-ray pulses, potentially making time resolved CXDI studies of molecular dynamics possible [3–7].

In CXDI, the object is illuminated with coherent x rays and its far-field diffraction pattern is recorded without any optic [3,8–10]. From this diffraction pattern, the wave field behind the object is reconstructed by iteratively solving the phase problem [8,11–14]. Three-dimensional imaging is possible by recording a (tomographic) series of diffraction patterns [9,15–18]. Coherent illumination of the object is crucial to this technique, and the coherent dose on the sample determines the spatial resolution. As the coherent flux at modern synchrotron radiation sources is limited, CXDI experiments require long exposure times, and the spatial resolutions obtained so far have been similar to those of direct imaging techniques, lying in the range of a few 10 nm.

In this Letter, we report on a CXDI experiment with nanofocused illumination, from which the small gold particle under investigation was reconstructed with 5 nm spatial resolution. As a result of the nanofocusing, the coherent flux on the sample was efficiently increased, reducing considerably the exposure time at high spatial resolution. This opens the way to combine scanning microscopy and CXDI to obtain a spatial resolution well beyond that of each technique taken by itself [19–22] and

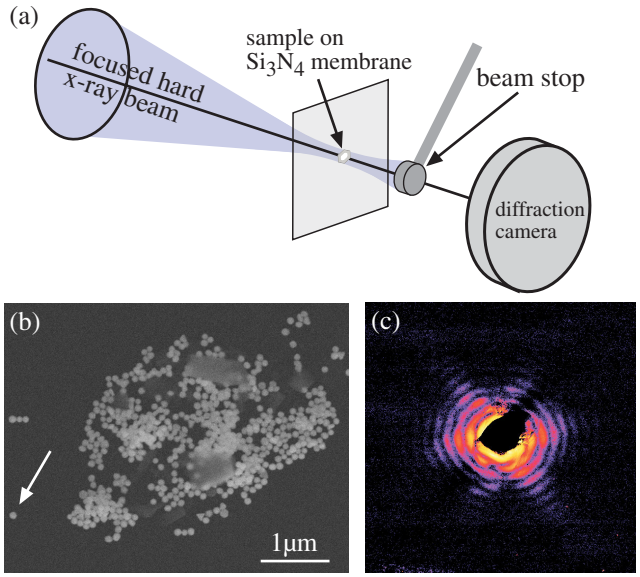

FIG. 1 (color online). (a) Schematic sketch of the coherent diffraction imaging setup with nanofocused illumination. (b) Scanning electron micrograph of gold particles (diameter $\approx$100 nm) deposited on a Si_3N_4 membrane. (c) Diffraction pattern (logarithmic scale) recorded of the single gold particle pointed to by the arrow in (b) and illuminated by a hard x-ray beam with lateral dimensions of about 100×100 nm^2. The maximal momentum transfer, both in horizontal and vertical direction, is $q = 1.65$ nm^{-1}.

is crucial to single particle diffraction experiments at future free-electron laser sources [4].

The nano-CXDI experiment was realized with our hard x-ray microscope set up at beam line ID13 of the European Synchrotron Radiation Facility (ESRF). A schematic sketch of the experimental setup is shown in Fig. 1(a): The sample is fully illuminated by a diffraction limited, nanofocused hard x-ray beam. The directly transmitted beam is blocked by a beam stop, and the diffraction pattern of the object is recorded in forward scattering geometry on a diffraction camera [cf. Fig. 1(a)]. This diffraction pattern is then used to reconstruct the projected electron density of the object by iterative schemes.

The x rays from an in-vacuum undulator source were monochromatized with a channel-cut Si (111) monochromator at an energy of $E = 15.25$ keV (wavelength $\lambda = 0.813$ Å). Two crossed refractive nanofocusing lenses (NFLs) [23,24] were used in the scanning microscope that was set up at a distance of $L_1 = 44$ m from the source. In the focus, a beam size slightly larger than 100×100 nm^2 was measured using a knife-edge technique. The flux in this beam exceeded 10^8 ph/s yielding a gain in intensity of $g = 10^4$.

The sample, a single gold nanoparticle supported by a Si_3N_4 membrane, was placed in the nanofocus. Figure 1(b) shows a cluster of such particles on a Si_3N_4 membrane of 50 nm thickness. The white arrow in Fig. 1(b) points to the gold particle investigated here. It was located by fluorescence mapping. In this first proof-of-principle nano-CXDI experiment, we chose a gold particle because of its comparably large scattering cross section and its relative radiation hardness.

A diffraction pattern of the sample was recorded with 10 one-minute exposures on a diffraction camera (FReLoN 4M, 50 μm pixel size) located at a distance of 1250 mm behind the sample. As the beam stop was too large to cover the central diffraction maximum, alone, it was moved up and down to record the inner parts of the diffraction pattern in several steps. In Fig. 1(c), the combined diffraction pattern is shown. It is oversampled by about a factor of 20 in both directions and has inversion symmetry except for a reduction in intensity in the upper right quadrant due to the support of the beam stop.

The diffraction pattern in Fig. 1(c) was used to reconstruct the gold particle using the hybrid input-output (HIO) method [11,25] together with the so-called shrink-wrap algorithm [26]. We performed 200 independent reconstructions out of which 191 converged to similar enantiomorphs [27] of the gold particle [cf. Fig. 2(a)]. These were combined to an average reconstruction shown in Fig. 2(b). From the root mean square variation of the reconstructions, the relative error of the electron density can be estimated. A horizontal section through the center of the particle is shown in Fig. 2(c). The reconstruction error is nearly constant over the whole object, and its border has a fuzziness of one to two pixels, corresponding to a spatial

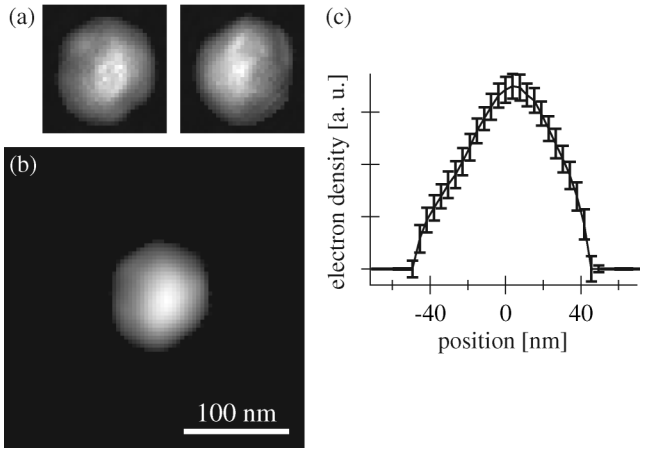

FIG. 2. (a) Two individual reconstructions of the gold particle using the HIO algorithm, a left- and a right-handed one. To obtain the average particle shape from a series of reconstructions with random initial phases, the right-handed reconstructions were inverted and averaged together with the left-handed ones. (b) Reconstructed projected electron density of the gold nanoparticle shown in Fig. 1(b) after averaging the series of reconstructions. (c) Horizontal section through the center of the particle shown in (b). The error bars indicate rms variations in the density for the series of independent reconstructions.

resolution of 3.8 to 7.6 nm, respectively. Evaluating the phase retrieval transfer function [9,10] by determining the highest momentum transfer for which the phase correlation in the reconstruction is above 10%, a corresponding half period of 4.3 nm is obtained, in agreement with the real space estimate for the spatial resolution given above.

The spatial resolution of CXDI is effectively limited by the strong decay of the diffraction intensity with increasing scattering vector $\vec{q}$. For a generic object, the diffraction intensity decays with a power law $q^{-\alpha}$ ($\alpha \approx 4$) [28]. Thus, an increase in resolution by 1 order of magnitude for a given experimental setup requires an increase in dose by about 4 orders of magnitude.

The total number of photons D_c in the coherence volume available at a given source, however, is bounded from above by

$$D_c = F_c T = \mathrm{Br}\lambda^2 \frac{\Delta E}{E} T,$$

where F_c is the coherent flux, Br is the brilliance of the x-ray source, λ is the wavelength of the x rays, $\Delta E/E$ the degree of monochromaticity, and T the exposure time. For storage ring based x-ray sources, the brilliance Br can not be significantly increased much further. In addition, to approach nanometer resolution and below, the requirements on the wavelength λ and the monochromaticity $\Delta E/E$ become more and more stringent, reducing the maximal coherent flux. One way to increase the dose on the sample and thus the spatial resolution is to increase the exposure time T. This scheme has been followed in most high resolution experiments, so far. However, the gain in

resolution is very small, as the exposure time grows with the fourth power of the resolution.

Much more can be gained by efficiently focusing the coherent flux onto a small sample. With increasing gain g of the focusing setup, the diffraction intensity is increased linearly, improving the spatial resolution by a factor $g^{1/\alpha}$. With the gain of 10^4 given in our setup, the spatial resolution is improved by one full order of magnitude. For comparison, in order to obtain the same result with the unfocused beam, the exposure time would have to be increased by a factor 10^4 to more than two months.

Figure 1(c) shows a high visibility of the interference fringes, thus demonstrating a high degree of coherence of the illumination of the object. In the following, the focusing conditions required for nano-CXDI are investigated. The longitudinal coherence length $l_l = \lambda^2/\Delta\lambda$ is about half a micrometer for the experimental conditions ($E =$ 15.25 keV and Si (111) monochromaticity $\Delta E/E = 1.4 \times 10^{-4}$). Although refractive optics have a strong dispersion ($\Delta f/f = 2\Delta E/E$), the chromatic aberration is more than 1 order of magnitude smaller than the depth of focus, i.e., 3.6 μm vs 83 μm and 6.4 μm vs 153 μm in horizontal and vertical direction, respectively, and is thus negligible. In addition, the path length differences in the small object (< 100 nm) are all much smaller than l_l for all diffraction angles. Therefore, the longitudinal coherence is largely sufficient for the current experiment and would even meet the requirements for CXDI with up to atomic resolution.

To estimate the lateral coherence in the beam, we calculate the mutual intensity $J(\vec{r}, \vec{r}')$ [29] in the focal plane, assuming a Gaussian incoherent source that is focused by two ideal crossed nanofocusing refractive x-ray lenses. It is given by

$$J(\vec{r}, \vec{r}') = I_0 e^{-[(\vec{r}^2+\vec{r}'^2)/(2\times 2\sigma_b^2)]} e^{-[(\vec{r}-\vec{r}')^2/(2\times\sigma_{l_t}^2)]}, \quad (1)$$

where $\vec{r}$ and $\vec{r}'$ are both coordinates in the focal plane, I_0 is the intensity in the focus on the optical axis, σ_b is the root mean square (rms) width of the intensity distribution in the focus, and σ_{l_t} is an rms distance in which the correlations between the amplitudes at different positions $\vec{r}$ and $\vec{r}'$ decay. It can be regarded as an rms lateral coherence length in the focus.

$$\sigma_b = \frac{\sqrt{b_{\text{geo}}^2 + d_t^2}}{2\sqrt{2\ln 2}} \quad \text{and} \quad \sigma_{l_t} = \frac{2d_t}{2\sqrt{2\ln 2}}\sqrt{1 + \frac{d_t^2}{b_{\text{geo}}^2}}$$

depend on the full width at half maximum (FWHM) geometric image size b_{geo} of the source and the FWHM diffraction limit d_t of the focusing geometry [23,30].

In a diffraction experiment, the pattern is determined by the x-ray amplitudes at the sample position and not by their intensity. Thus, here, the width of the beam in terms of amplitudes is relevant. It is $\sqrt{2}$ times wider than that of the intensity for a Gaussian beam, i.e., $b_{\text{ampl}} = \sqrt{2}b = \sqrt{2} \times 2\sqrt{2\ln 2}\sigma_b \approx 150$ nm. For increasing lateral coherence length $l_t = 2\sqrt{2\ln 2} \times \sigma_{l_t}$ compared to the beam width b_{ampl}, the beam becomes more and more coherent. Figure 3 depicts both the beam size b_{ampl} and the lateral coherence length l_t as a function of the geometric image size b_{geo} of the source.

If b_{geo} is large compared to d_t, the beam size b_{ampl} is dominated by geometric optics. In that case, the lateral coherence length l_t is about 2 times d_t and smaller than the beam size: the beam illuminates the sample incoherently. If, on the other hand, b_{geo} is negligible compared to d_t, the beam size b_{ampl} approaches $\sqrt{2}d_t$, and the lateral coherence length l_t diverges: the sample is coherently illuminated. The crossover from the focusing regime with coherent illumination to that with incoherent illumination occurs when b_{ampl} equals l_t, i.e., $b_{\text{geo}} = \sqrt{2}d_t$. Therefore, for diffraction limited beams, the lateral coherence length is larger than the focus size, and thus the illumination is coherent to a high degree.

In the experiment described here, both the horizontal and the vertical focus fall into the regime of high coherence, i.e., $l_{t_h} = 180$ nm and $l_{t_v} = 360$ nm (shown as circles and rectangles in Fig. 3, respectively). This explains why the fringe visibility is high in Fig. 1(c) for the object with a diameter smaller than 90 nm.

In practice, the optics are not free of spherical aberrations, leading to a non-Gaussian illumination of the object. The deviations of the nanofocusing lenses from the ideal shape can be estimated from the beam shape in the far field [31]. Wave optical calculations of the whole setup including aberrations suggest that the wave front in the focus (central maximum) is laterally larger in size but flat in the phase for the present optics. This is in good agreement with the fact that the reconstruction of the diffraction pattern works reliably when assuming a flat, undistorted wave front at the sample position.

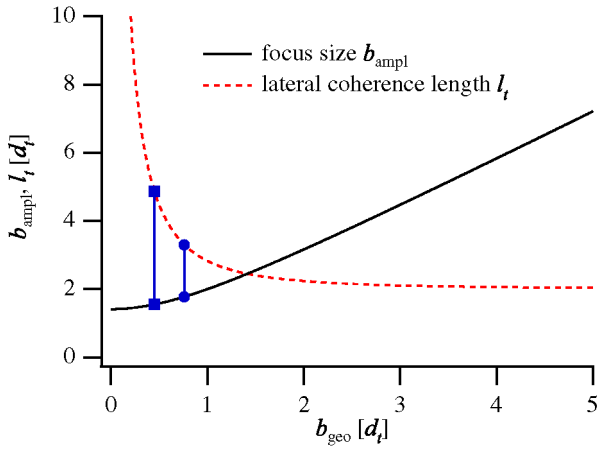

FIG. 3 (color online). Beam size b_{ampl} of the x-ray amplitude and lateral coherence length l_t as a function of the geometric image size b_{geo} of the source. All quantities are in units of the diffraction limit d_t (size of Airy disc).

From the current experiment, it is possible to estimate the spatial resolution that is achievable with nano-CXDI. To further improve the resolution compared to the given experiment, the coherent flux density on the sample needs to be increased further, e.g., by more efficient focusing to smaller foci. By improving refractive optics in terms of image quality and transmission, the gain g could be increased further by about 2 orders of magnitude. In addition, by optimally matching the lateral coherence length of the incident beam to the aperture of the optic, e.g., by appropriate prefocusing, another order of magnitude can be gained. With these 3 orders of magnitude attained in flux density, the resolution could be pushed to below 1 nm for strong and radiation-hard scatterers. Further improvements in the spatial resolution would require an increase in brilliance of the source that could be provided by an energy recovery linac (ERL) [32]. As the dose on the sample is increased further, radiation damage becomes more and more relevant, eventually limiting the spatial resolution, in particular, for many organic materials [28].

Besides investigating small isolated objects, it is possible to investigate extended objects by combining scanning microscopy with CXDI [19–22]. This technique, also called ptychography, has many advantages over conventional CXDI. The sample is scanned with spatially confined illumination, e.g., a nanofocused hard x-ray beam. At each position of the scan, a full diffraction pattern is recorded. The scanning steps are chosen such that the illumination at a given point has an overlap with that of neighboring scan points. In this way, applying a similar iterative reconstruction scheme to the whole set of diffraction patterns, ambiguities in the reconstruction are avoided, such as the enantiomorph problem or a positional ambiguity of the object. In addition, the object can be laterally extended and does not need to be placed onto a featureless transparent support. The total dose required by ptychography to image a given field of view, however, does not depend on the focus size. The gain in flux density obtained by reducing the focus size is compensated by the number of scanning steps required to scan the object. Thus, an increase in spatial resolution by focusing can only be obtained by reducing the field of view. Regardless of this, ptychography is an attractive method to combine both real and reciprocal space methods to improve the spatial resolution beyond that of conventional x-ray microscopy.

To study the structure of small particles at x-ray free-electron laser sources, focusing the laser pulse is crucial to obtain high spatial resolution, as the diffraction pattern needs to be recorded with a single pulse and a limited number of photons.

We wish to thank I. Snigireva for the SEM images of the sample. This work is supported by the German Ministry of Education and Research (BMBF) under Grant No. 05KS7OD1 and by VI-203 of the Impuls- und Vernetzungsfonds (IVF) of the Helmholtz-Society.

[1] *Proceedings of the 8th International Conference on X-Ray Microscopy*, IPAP Conference Series Vol. 7, edited by Y. Kagoshima (IPAP, Tokyo, 2006).
[2] While there is still room for improvement of these optics, focusing to dimensions smaller than 10 nm becomes increasingly challenging [C. Bergemann, H. Keymeulen, and J. F. van der Veen, Phys. Rev. Lett. **91**, 204801 (2003); C. G. Schroer and B. Lengeler, Phys. Rev. Lett. **94**, 054802 (2005); H. C. Kang *et al.*, Phys. Rev. Lett. **96**, 127401 (2006); H. Yan *et al.*, Phys. Rev. B **76**, 115438 (2007)].
[3] H. N. Chapman *et al.*, Nature Phys. **2**, 839 (2006).
[4] R. Neutze *et al.*, Nature (London) **406**, 752 (2000).
[5] *XFEL, The European X-Ray Free-Electron Laser (TDR)*, edited by M. Altarelli *et al.* (DESY, Hamburg, 2006).
[6] H. N. Chapman *et al.*, Nature (London) **448**, 676 (2007).
[7] M. J. Bogan *et al.*, Nano Lett. **8**, 310 (2008).
[8] J. Miao, P. Charalambous, J. Kirz, and D. Sayre, Nature (London) **400**, 342 (1999).
[9] H. N. Chapman *et al.*, J. Opt. Soc. Am. A **23**, 1179 (2006).
[10] D. Shapiro *et al.*, Proc. Natl. Acad. Sci. U.S.A. **102**, 15343 (2005).
[11] J. R. Fienup, Appl. Opt. **21**, 2758 (1982).
[12] I. K. Robinson *et al.*, Phys. Rev. Lett. **87**, 195505 (2001).
[13] I. A. Vartanyants and I. K. Robinson, J. Phys. Condens. Matter **13**, 10593 (2001).
[14] G. J. Williams, H. M. Quiney, A. G. Peele, and K. A. Nugent, Phys. Rev. B **75**, 104102 (2007).
[15] J. Miao *et al.*, Phys. Rev. Lett. **89**, 088303 (2002).
[16] G. J. Williams, M. A. Pfeifer, I. A. Vartanyants, and I. K. Robinson, Phys. Rev. Lett. **90**, 175501 (2003).
[17] J. Miao *et al.*, Phys. Rev. Lett. **97**, 215503 (2006).
[18] M. A. Pfeifer *et al.*, Nature (London) **442**, 63 (2006).
[19] J. M. Rodenburg and H. M. L. Faulkner, Appl. Phys. Lett. **85**, 4795 (2004).
[20] H. M. L. Faulkner and J. M. Rodenburg, Phys. Rev. Lett. **93**, 023903 (2004).
[21] J. M. Rodenburg *et al.*, Phys. Rev. Lett. **98**, 034801 (2007).
[22] P. Thibault *et al.*, Science **321**, 379 (2008).
[23] C. G. Schroer *et al.*, Appl. Phys. Lett. **82**, 1485 (2003).
[24] C. G. Schroer *et al.*, Appl. Phys. Lett. **87**, 124103 (2005).
[25] For each reconstruction, 5000 iterations were performed. Periodically, the algorithm was switched between 60 error reduction (ER) and 40 HIO cycles. In real space, a support and a positivity constraint were used. The support was updated by the shrink-wrap algorithm.
[26] S. Marchesini *et al.*, Phys. Rev. B **68**, 140101(R) (2003).
[27] From a centro-symmetric diffraction pattern, the object and its inversion can not be distinguished. Therefore, the HIO algorithm reconstructs both enantiomorphs of the gold particle with the same frequency.
[28] S. Marchesini *et al.*, Opt. Express **11**, 2344 (2003).
[29] M. Born and E. Wolf, *Principles of Optics* (Cambridge University Press, Cambridge, 1999).
[30] B. Lengeler *et al.*, J. Synchrotron Radiat. **6**, 1153 (1999).
[31] H. M. Quiney *et al.*, Nature Phys. **2**, 101 (2006).
[32] D. H. Bilderback *et al.*, J. Synchrotron Radiat. **10**, 346 (2003).